의학박사 학위논문

Intraocular distribution and kinetics of intravitreally injected non-biodegradable nanoparticles in rabbits

백색 가토의 유리체강내로 주입된 비생분해성 나노입자의 안구내 분포와 동력학

2016 년 8 월

서울대학교 대학원

의학과 안과학 전공

하 승 민

Intraocular distribution and kinetics of intravitreally injected non-biodegradable nanoparticles in rabbits

지도교수 박 규 형

이 논문을 의학박사 학위논문으로 제출함
2016 년 4 월

서울대학교 대학원
의학과 안과학 전공
하 승 민

하승민의 의학박사 학위논문을 인준함
2016 년 6 월

위 원 장	김 용 식	(인)
부위원장	박 규 형	(인)
위 원	허 장 원	(인)
위 원	우 세 준	(인)
위 원	조 영 준	(인)

Abstract

Intraocular distribution and kinetics of intravitreally injected non-biodegradable nanoparticles in rabbits

Seungmin Ha

Medicine, Ophthalmology

The Graduate School

Seoul National University

Introduction: Recently, intravitreal injection of large protein drugs has been used for the treatment of many retinal diseases. Although molecular weight is the main factor in determining the kinetics, the exact mechanisms underlying drug delivery and intraocular distribution and elimination of these drugs has not been elucidated. Efforts have been made to enhance drug delivery to ocular tissues using various kinds of drug delivery systems, including nanoparticles. This study was performed to analyze the intraocular distribution and kinetics of intravitreally injected non-biodegradable nanoparticles in rabbit eyes, to help understand the intraocular

biodistribution of intravitreous materials and drugs.

Methods: Four kinds of fluorescent non-biodegradable polystyrene nanoparticles were used in this study: 25 nm and 250 nm diameter nanoparticles to investigate the intraocular distribution and elimination pathways of nanoparticles and intraocular kinetics of nanoparticles, and 50 nm and 200 nm diameter nanoparticles to investigate the intraocular kinetics of nanoparticles. A 0.034 ml mixture of 25 nm nanoparticles and 250 nm nanoparticles (1:1) was injected intravitreally into 24 eyes of 12 New Zealand white rabbits. Four eyes were enucleated at each time point (1 hour, 1 day, 7 days, 14 days, 21 days, and 30 days after the injection) and immediately frozen at -80 ℃. Fluorescence microscopic imaging was performed on one eye at each time point. Fluorescence microscopic imaging of the cross section of each frozen enucleated eyeball was performed using a custom-built laser-scanning confocal system modified for wide-field imaging before it began to melt. Intraocular distribution of nanoparticles was analyzed serially with software at each time point. The other three eyes from each time point were used for fluorescence measurements. A 10-fold diluted solution of 50 nm nanoparticles was injected intravitreally into 15 right eyes of 15 New Zealand white rabbits and a 100-fold diluted solution of 200 nm nanoparticles was injected intravitreally into 15 right eyes of 15 New Zealand white rabbits. Three eyes per solution group per time point were enucleated for fluorescence measurements at 1 hour, 1 day, 7 days, 14 days, and 30 days after the

injection and immediately frozen at -80 ℃. The optical density of fluorescence was determined using a fluorescence microplate reader after the separation of frozen vitreous, aqueous humor, and retina, and the concentration of nanoparticles in each sample was determined.

Results: Serial imaging of the intraocular distribution of nanoparticles showed that the intensity of fluorescence did not decrease in the vitreous over time and the injected nanoparticles moved posteriorly to the retina from 7 days after the injection. However, the nanoparticles could not penetrate into the deeper retinal structures and accumulated on the internal limiting membrane. Furthermore, the nanoparticles moved anteriorly in the vitreous at 1 hour and 1 day post-injection, and the fluorescence increased in the anterior chamber until 14 days after the injection and it decreased thereafter. In the image of the eye that had been enucleated 21 days after the injection, we found that the 25 nm nanoparticles moved across the ciliary body into the choroid and episcleral space. Overall, the concentration of nanoparticles in the vitreous did not change at all the measured time points, irrespective of sizes. In the aqueous humor, the concentration of 50 nm and 200 nm nanoparticles did not increase after the 1-day time point and the 25 nm and 250 nm nanoparticles did not increase after the 7-day time point. Nanoparticles were detected in the retinal tissue.

Conclusion: The result of the intraocular distribution, changes in concentration, and elimination pathways of various-sized non-biodegradable nanoparticles may be used

as basic data in the studies of intraocular drug delivery and pharmacokinetics using nanoparticles in the future. It might also indicate the possible mechanisms underlying intraocular elimination and movement of intravitreally injected drugs, which are currently used to treat retinal diseases.

……....

Keywords: nanoparticle, intravitreal injection, distribution, kinetics

Student Number: 2010-30553

Contents

List of Tables

List of Figures

Introduction

Age-related macular degeneration (AMD) is the leading cause of visual loss in individuals over the age of 50 years in developed countries. Neovascular AMD is less common, affecting only 10% of AMD patients. However, it is more likely to lead to significant visual loss. Without treatment, the condition causes irreversible damage to the retinal layers and yields central visual loss.[1] Diabetic macular edema is the major cause of vision loss associated with diabetic retinopathy. The overall prevalence of diabetic macular edema is 6.81% in individuals with diabetes worldwide,[2] accounting for 12% of new cases of blindness annually.[3] Studies of the natural history of diabetic macular edema suggest that 24% of eyes with diabetic macular edema will lose at least three lines of vision within 3 years.[4] Branch and central retinal vein occlusion (RVO) are among the most common retinal vascular diseases and are often associated with moderate to severe vision loss.[5] Macular edema is the main cause of visual impairment in central retinal vein occlusion (CRVO) and branch retinal vein occlusion (BRVO).[6,7]

Intravitreal injection of anti-VEGF agents and triamcinolone acetonide has become the mainstay of treatment in these sight-threatening retinal diseases as it not only reduces the exudative changes but also provides significant improvements in visual function.[8–24] Although direct intravitreal injections provide high

concentrations of drugs to the retina, the short half-life of this method necessitates frequent repeated administration.[25] The intravitreal half-lives of bevacizumab, ranibizumab, aflibercept, and triamcinolone acetonide in previous studies varied from 2.75 to 24 days.[26–43] Therefore, patients are constantly exposed to substantial complications including intravitreal hemorrhage, endophthalmitis, retinal detachment, cataract, and opening of the sclerotomy site.[44,45] Moreover, patients may not comply with such regimens, which might further hinder treatment. The development of excellent drug delivery systems is essential to deliver therapeutic levels of drugs to the posterior segment of the eye, and research on the distribution and kinetics of intravitreally injected drugs plays an important role. Although molecular weight is the main factor determining the kinetics, the exact mechanism of drug delivery and intraocular distribution and elimination is still obscure.

Nanotechnology involves the creation and use of materials and devices at the scale of intracellular structures. The molecules, systems, and constructs involved are often under 100 nm.[46] The application of nano-scale technologies to the practice of medicine will profoundly alter our approach to the diagnosis, treatment, and prevention of disease.[47] Nanotechnology has also been used in the fields of ophthalmology. Various kinds of drug-loaded nanoparticles have been studied in experiments for the treatment of glaucoma, posterior capsular opacification after cataract surgery, vitreoretinal diseases, corneal diseases, optic nerve crush injury,

and uveitis.[48–63]

However, only a few studies have analyzed the distribution and kinetics of nanoparticles, especially non-biodegradable nanoparticles.[64–66] Inokuchi et al. reported that the delivery efficiency of fluorescent probes from dropped liposomes to the mouse retina was extensively improved by reducing their particle size (<600 nm) and cholesterol content. However, fluorescein isothiocyanate (FITC)-labeled polystyrene particles and coumarin-6-incorporated lipid emulsions showed an insufficient effect on retinal delivery in mice even if their size was controlled at 100 nm when they were administered topically using eyedrops.[66] Amrite et al. suggested that the particle size of the delivery system plays an important role in the observed retinal drug levels after periocular administration. The 20 nm particles are transported across the sclera to a minor degree; however, there is no significant transport across the sclera-choroid-RPE.[64] These reports are about topical or periocular administration. Sakurai et al. studied the kinetics of intravitreally injected suspensions of polystyrene nanoparticles (2 μm, 200 nm, and 50 nm in diameter) containing a fluorescein derivative in rabbits. They reported that the elimination half-life from the vitreous cavity correlated well with the particle diameter.[65]

Evaluation of the intraocular distribution, elimination, and pharmacokinetics of large molecules is limited owing to the spontaneous degradation of currently available protein drugs. Therefore, non-biodegradable nanoparticles are thought to

be more suitable to evaluate the intraocular distribution, elimination, and pharmacokinetics in the vitreous. Moreover, they can provide useful information on nanoparticle drug delivery systems, which is imperative considering that nanoparticles are in the spotlight as nanocarriers for drug delivery. Hence, this study was performed to analyze the intraocular distribution and kinetic profiles of intravitreally injected non-biodegradable nanoparticles in rabbit eyes by performing fluorescence microscopic imaging of enucleated eyes and measuring the fluorescence of the vitreous, aqueous humor, and retina using a fluorescence microplate reader, in order to help understand the intraocular biodistribution of intravitreous materials and drugs.

Materials and Methods

1. Preparation of nanoparticles

Four kinds of nanoparticles were used in this study: 25 nm and 250 nm diameter nanoparticles to investigate the intraocular distribution and elimination pathways of nanoparticles and intraocular kinetics of nanoparticles, and 50 nm and 200 nm diameter nanoparticles to investigate the intraocular kinetics of nanoparticles.

The micromer-redF (25 nm red fluorescent non-biodegradable polystyrene particle, micromod Partikeltechnologie GmbH, Rostock, Germany) has an excitation wavelength of 552 nm and emission wavelength of 580 nm. The micromer-greenF (250 nm green fluorescent non-biodegradable polystyrene particle, micromod Partikeltechnologie GmbH, Rostock, Germany) has an excitation wavelength of 475 nm and emission wavelength of 510 nm. In the micromer-redF solution, nanoparticles with a diameter of 25 nm were packaged as a 10 mg/ml ($1.2x10^{14}$ particles/mg) aqueous suspension and the concentration was $1.2x10^{15}$ particles/ml. In the micromer-greenF solution, nanoparticles with a diameter of 250 nm were packaged as a 25 mg/ml ($1.2x10^{11}$ particles/mg) aqueous suspension and the concentration was $3x10^{12}$ particles/ml.

The Fluoresbrite Yellow Green Microspheres (Polysciences, Inc., Warrington, PA,

USA) have excitation and emission spectra similar to fluorescein isothiocyanate (FITC) with an excitation wavelength of 441 nm and emission wavelength of 485 nm. In Fluoresbrite YG Microspheres 0.05 μm solution, nanoparticles with a diameter of 50 nm were packaged as a 2.5% aqueous suspension and the concentration was $3.64x10^{14}$ particles/ml. In Fluoresbrite YG Microspheres 0.20 μm solution, nanoparticles with a diameter of 200 nm were packaged as a 2.5% aqueous suspension and the concentration was $5.68x10^{12}$ particles/ml. In a preliminary experiment, we found that the nanoparticles were aggregated after we injected an undiluted aqueous suspension into the vitreous. Therefore, we prepared a 10-fold diluted solution of Fluoresbrite YG Microspheres 0.05μm and 100-fold diluted solution of Fluoresbrite YG Microspheres 0.20μm for intravitreal injection.

The nanoparticles are negatively charged and spherical in shape.

2. Preparation of animal experiment

After approval from the Seoul National University Bundang Hospital Institutional Animal Care and Use Committee, experiments were conducted with procedures adhering to the guidelines from the Association for Research in Vision and Ophthalmology for animal use in research. A total of 42 healthy New Zealand white rabbits weighing 1.5-2 kg were used for the study. Rabbits were anesthetized with an intramuscular injection of 15 mg/kg tiletamine hydrochloride/zolazepam

hydrochloride (Zoletil, Virbac laboratories, CarrosCedex, France) and 5 mg/kg of xylazine hydrochloride (Rompun, Bayer Healthcare, Seoul, Korea). After dilation with 0.5% tropicamide and 0.5% phenylephrine hydrochloride eyedrops (Mydrin-P, Santen Pharmaceutical Co., Osaka, Japan), topical anesthesia was induced using 1% proparacaine hydrochloride eyedrops (Alcaine, Alcon laboratories, Inc., Fort Worth, TX, USA). The periocular area was disinfected with 10% povidone iodine solution and the eye was opened with a speculum. After applying 5% povidone iodine eyedrops on the conjunctiva, all procedures were conducted aseptically.

3. Intravitreal injection

Using a 30-gauge needle, a 0.034 ml mixture of 25 nm and 250 nm nanoparticles solution (1:1) was injected intravitreally, 2 mm behind the limbus in the superotemporal quadrant in 24 eyes of 12 rabbits. Using a 30-gauge needle, a 0.05 ml solution of 50 nm nanoparticles was injected intravitreally, 2 mm behind the limbus in the superotemporal quadrant in 15 right eyes of 15 rabbits and a 0.05 ml solution of 200 nm nanoparticles was injected intravitreally in 15 right eyes of 15 rabbits. At the end of the procedure, a broad-spectrum antibiotic ointment was applied to the eye.

4. Enucleation and storage of eye

To investigate the intraocular distribution and kinetics of 25 nm and 250 nm nanoparticles, two rabbits were sacrificed at each of the following six time points: 1hour, 1 day, 7 days, 14 days, 21 days, and 30 days after intravitreal injection. Both eyes were enucleated and immediately frozen at -80 ℃.

To investigate the intraocular kinetics of 50 nm and 200 nm nanoparticles, three rabbits per solution group were sacrificed at each of the following five time points: 1hour, 1 day, 7 days, 14 days, and 30 days after intravitreal injection. The right eye was enucleated and immediately frozen at -80 ℃.

5. Fluorescence microscopic imaging of enucleated eye

Fluorescence microscopic imaging of enucleated frozen eye samples was performed using a custom-built laser-scanning confocal system modified for wide-field imaging.[67,68] Continuous-wave laser modules with output wavelengths at 488 nm (MLD488, Cobolt) and 561 nm (Jive, Cobolt) were used as excitation sources for green fluorescent 250 nm diameter nanoparticles and red fluorescent 25 nm diameter nanoparticles, respectively. Fluorescence emission signals were detected by multialkali photocathode photomultiplier tubes (R9110, Hamamatsu, Japan). Green and red fluorescence signals were detected through emission filters with a

bandpass at 500–550nm (FF02-525/50, Semrock) and 581.5–618.5 nm (FF01-600/37, Semrock), respectively. Collinearly aligned excitation laser beams were raster-scanned by a rotating polygonal mirror (MC-5, Lincoln Laser, USA) and a galvanometer based scanning mirror (6230H, Cambridge technology, USA), and then delivered to the sample via relay optics. The imaging platform was designed to provide various fields of view from 0.17 mm to 13 mm by replacing the relay optics. In this experiment, 2.5 mm and 13 mm fields of view were used, respectively, for high and low magnification. The cross section images of the whole eyeball were constructed by mosacing multiple images acquired with the low magnification setup with 13 mm field of view by using Photoshop (Adobe).

The cross section of a frozen eyeball was prepared for imaging by gradually cutting off a small portion of the eyeball horizontally with a cryotome from the top. To observe the cross section at the similar position in each eyeball, for comparison, eyeball sections of similar thickness were cut from the top. Dry ice blocks were stacked surrounding the sample during the imaging, to prevent tissue deformation and leakage of the aqueous humor.

6. Separation of aqueous humor, vitreous, and retina

The frozen vitreous, aqueous humor, and retina were subsequently separated from the eye. Separated samples were placed in 1.7 ml Eppendorf tubes and stored at -

80 ℃ until required for the optical density assay.

Before analysis, the frozen vitreous and aqueous humor samples were defrosted and homogenized by an ultrasonicator for 30 seconds at 4 ℃. The frozen retina was lysed completely by adding CelLytic™ MT Mammalian Tissue Lysis/Extraction Reagent (10 ml/g of tissue) (Sigma, Saint Louis, MO, USA).

7. Optical density measurement of fluorescence

Each sample was aliquoted in triplicate in a 96-well microplate (100 μl/well). The optical density of 50 nm and 200 nm nanoparticles was measured with an excitation wavelength of 441 nm and emission wavelength of 485 nm in a fluorescence microplate reader (SpectraMax Gemini EM, Molecular Devices, Sunnyvale, CA, USA). The optical density of 25 nm nanoparticles was measured with an excitation wavelength of 552 nm and emission wavelength of 580 nm and 250 nm nanoparticles with an excitation wavelength of 475 nm and emission wavelength of 510 nm.

We prepared the standard curves for 50 nm and 200 nm nanoparticles by performing 12 dilutions of 1/2, 1/5, 1/10, 1/20, 1/50, 1/100, 1/200, 1/500, 1/1000, 1/2000, 1/5000, and 1/10000 of the original aqueous suspension and measuring the optical density in the same plate. We prepared the standard curves for 25 nm and 250 nm nanoparticles by performing 8 dilutions of 1/3, 1/15, 1/75, 1/375, 1/1875,

1/9375, 1/46875, and 1/234375 of the original aqueous suspension and measuring the optical density in the same plate.

8. Calculation of the concentration of nanoparticles in aqueous humor, vitreous, and retina

We determined the concentration (number of particles/ml) of each sample using their optical density, number of particles/mg, and standard curve.

Results

Data were collected from 24 eyes of 12 rabbits injected with 25 nm and 250 nm nanoparticles and from 30 eyes of 30 rabbits injected with 50 nm and 200 nm nanoparticles. There was no evidence of ocular inflammation or other adverse events related to intravitreal nanoparticle injection.

1. Fluorescence microscopic imaging

Serial imaging of the intraocular distribution of nanoparticles showed that the intensity of fluorescence did not decrease in the vitreous over time. It also showed that the intravitreally injected nanoparticles moved posteriorly to the retina from 7 days post-injection and numerous nanoparticles were observed in front of the retina at 30 days post-injection (Figure 1). However, we found that nanoparticles could not penetrate into the deeper retinal structures and accumulated on the internal limiting membrane (Figure 2). The serial imaging also showed that the nanoparticles moved anteriorly in the vitreous at 1 hour and 1 day post-injection and the fluorescence increased in the anterior chamber until 14 days after the injection and it decreased thereafter (Figure 1). In the image of the eye that had been

enucleated 21 days after the injection, we found that the 25 nm nanoparticles moved across the ciliary body into the choroid and episcleral space (Figure 3).

2. Intraocular kinetics of nanoparticles

2-1. Standard curve

Two types of standard curves were made for the 50 nm nanoparticles ($y = 2x10^{-10}\chi+1.9801$, $R^2 = 0.9963$; $y = 3x10^{-10}\chi-26.375$, $R^2 = 0.9975$). The former was used for the aqueous humor and retina, which had a low optical density and the latter for the vitreous, which had a high optical density. For 200 nm nanoparticles, two types of standard curves were made ($y = 8x10^{-8}\chi+2.8655$, $R^2 = 0.9949$; $y = 9x10^{-8}\chi-3.3016$, $R^2 = 0.9992$). The former was used for the aqueous humor and retina, which had a low optical density and the latter for the vitreous which had a high optical density. Three types of standard curves were made for 25 nm nanoparticles ($y = 27965\chi+328.01$, $R^2 = 0.9958$; $y = 28427\chi+379.1$, $R^2 = 0.995$; $y = 28020\chi+429.44$, $R^2 = 0.9946$). The first was used for the aqueous humor, the second for the vitreous, and the third for the retina. A standard curve was also made for the 250 nm nanoparticles ($y = 5461.5\chi+137.49$, $R^2 = 0.9889$).

2-2. Optical density measurement of fluorescence

For 50 nm and 200 nm nanoparticles, the average optical density of fluorescence in the aqueous humor, vitreous, and retina at 1 hour, 1 day, 7 days, 14 days, and 30 days post-injection is shown in Table 1 (50 nm) and Table 2 (200 nm). For 25 nm and 250 nm nanoparticles, the average optical density of fluorescence in the aqueous humor, vitreous, and retina at 1 hour, 1 day, 7 days, 14 days, 21 days, and 30 days post-injection is shown in Table 3 (25 nm) and Table 4 (250 nm).

2-3. The concentration of nanoparticles in aqueous humor, vitreous, and retina

The concentration of nanoparticles in the vitreous ranged from 7.83×10^{11}/ml to 1.28×10^{12}/ml for 50 nm nanoparticles, 1.14×10^{9}/ml to 1.46×10^{9}/ml for 200 nm nanoparticles, 9.20×10^{12}/ml to 1.38×10^{13}/ml for 25 nm nanoparticles, and 2.17×10^{10}/ml to 3.68×10^{10}/ml for 250 nm nanoparticles. The concentration of 25 nm and 50 nm nanoparticles decreased somewhat over time, but maintained to 30 days post-injection. The concentration of 200 nm and 250 nm nanoparticles hardly changed after 1 hour post-injection. The concentration of nanoparticles in the aqueous humor was 1.02×10^{10}/ml at 1 hour and 5.34×10^{10}/ml at 1 day for 50 nm nanoparticles. It was 1.52×10^{7}/ml at 1 hour and 8.49×10^{6}/ml at 1 day for 200 nm nanoparticles. The concentration ranged from 3.76×10^{12}/ml to 5.96×10^{13}/ml for 25

nm nanoparticles and $4.60x10^{9}$/ml to $1.38x10^{10}$/ml for 250 nm nanoparticles. The concentration of nanoparticles after the injection did not increase after 1 day for 50 nm and 200 nm nanoparticles and 7 days for 25 nm and 250 nm nanoparticles. The concentration of nanoparticles in the retina ranged from $4.35x10^{9}$/ml to $4.17x10^{10}$/ml for 50 nm nanoparticles. The concentration was $3.16x10^{7}$/ml at 1 hour and $4.10x10^{7}$/ml at 14 days for 200 nm nanoparticles. The concentration ranged from $3.20x10^{12}$/ml to $4.36x10^{12}$/ml for 25 nm nanoparticles and $3.72x10^{9}$/ml to $1.48x10^{10}$/ml for 250 nm nanoparticles (Tables 1~4, Figure 4 and 5).

Table 1. The average optical density of fluorescence and the average concentration (particles/ml) of nanoparticles in the aqueous humor, vitreous, and retina at 1 hour, 1 day, 7 days, 14 days, and 30 days after intravitreal nanoparticle injection (50 nm). A: aqueous humor, V: vitreous, R: retina, O: average optical density, C: average concentration

		1h	1d	7d	14d	30d
A	O	4.02 ± 1.69	12.26 ± 18.86	1.50 ± 0.28	1.62 ± 0.15	1.95 ± 0.23
	C	$1.02x10^{10}$ ± $8.43x10^{9}$	$5.34x10^{10}$ ± $9.25x10^{10}$	0	0	$3.38x10^{8}$ ± $4.28x10^{8}$
V	O	283.23 ± 215.84	358.46 ± 8.75	330.79 ± 62.44	298.21 ± 9.51	208.61 ± 71.32
	C	$1.03x10^{12}$ ± $7.20x10^{11}$	$1.28x10^{12}$ ± $2.92x10^{10}$	$1.19x10^{12}$ ± $2.08x10^{11}$	$1.08x10^{12}$ ± $3.17x10^{10}$	$7.83x10^{11}$ ± $2.38x10^{11}$
R	O	10.33 ± 6.58	2.85 ± 0.18	4.28 ± 1.83	3.46 ± 2.16	8.09 ± 8.81
	C	$4.17x10^{10}$ ± $3.29x10^{10}$	$4.35x10^{9}$ ± $9.05x10^{8}$	$1.15x10^{10}$ ± $9.15x10^{9}$	$7.41x10^{9}$ ± $1.08x10^{10}$	$3.05x10^{10}$ ± $4.41x10^{10}$

Table 2. The average optical density of fluorescence and the average concentration (particles/ml) of nanoparticles in the aqueous humor, vitreous, and retina at 1 hour, 1 day, 7 days, 14 days, and 30 days after intravitreal nanoparticle injection (200 nm). A: aqueous humor, V: vitreous, R: retina, O: average optical density, C: average concentration

		1h	1d	7d	14d	30d
A	O	3.73 ± 2.76	2.94 ± 1.71	2.91 ± 1.11	1.08 ± 0.27	1.62 ± 0.47
	C	$1.52x10^7$ ± $2.63x10^7$	$8.49x10^6$ ± $1.47x10^7$	0	0	0
V	O	128.03 ± 74.75	127.58 ± 15.24	128.41 ± 8.31	114.68 ± 16.59	99.36 ± 21.39
	C	$1.46x10^9$ ± $8.31x10^8$	$1.45x10^9$ ± $1.69x10^8$	$1.46x10^9$ ± $9.23x10^7$	$1.31x10^9$ ± $1.84x10^8$	$1.14x10^9$ ± $2.38x10^8$
R	O	4.23 ± 1.00	3.26 ± 1.23	3.36 ± 0.85	4.44 ± 2.89	3.61 ± 1.07
	C	$3.16x10^7$ ± $5.47x10^7$	0	0	$4.10x10^7$ ± $7.10x10^7$	0

Table 3. The average optical density of fluorescence and the average concentration (particles/ml) of nanoparticles in the aqueous humor, vitreous, and retina at 1 hour, 1 day, 7 days, 14 days, 21days, and 30 days after intravitreal nanoparticle injection (25 nm).

A: aqueous humor, V: vitreous, R: retina, O: average optical density, C: average concentration

		1h	1d	7d	14d	21d	30d
A	O	305.83 ± 207.41	313.69 ± 74.98	516.76 ± 101.37	401.56 ± 150.40	296.21 ± 51.92	359.60 ± 103.76
	C	$3.76x10^{12}$ ± $2.44x10^{12}$	$4.16x10^{12}$ ± $7.23x10^{11}$	$5.96x10^{12}$ ± $7.99x10^{11}$	$4.92x10^{12}$ ± $1.25x10^{12}$	$4.00x10^{12}$ ± $5.54x10^{11}$	$4.60x10^{12}$ ± $9.70x10^{11}$
V	O	1868.94 ± 249.22	1760.66 ± 214.18	1579.46 ± 218.46	1389.41 ± 60.25	1066.02 ± 151.47	992.04 ± 86.52
	C	$1.38x10^{13}$ ± $1.34x10^{12}$	$1.33x10^{13}$ ± $1.20x10^{12}$	$1.24x10^{13}$ ± $1.22x10^{12}$	$1.14x10^{13}$ ± $1.20x10^{11}$	$9.60x10^{12}$ ± $9.60x10^{11}$	$9.20x10^{12}$ ± $6.04x10^{11}$
R	O	253.42 ± 37.05	226.70 ± 23.25	294.98 ± 37.63	294.99 ± 37.35	310.08 ± 22.98	342.01 ± 20.62
	C	$3.48x10^{12}$ ± $4.16x10^{11}$	$3.20x10^{12}$ ± $2.77x10^{11}$	$3.92x10^{12}$ ± $4.21x10^{11}$	$3.88x10^{12}$ ± $3.86x10^{11}$	$4.08x10^{12}$ ± $2.08x10^{11}$	$4.36x10^{12}$ ± $1.83x10^{11}$

Table 4. The average optical density of fluorescence and the average concentration (particles/ml) of nanoparticles in the aqueous humor, vitreous, and retina at 1 hour, 1 day, 7 days, 14 days, 21days, and 30 days after intravitreal nanoparticle injection (250 nm).

A: aqueous humor, V: vitreous, R: retina, O: average optical density, C: average concentration

		1h	1d	7d	14d	21d	30d
A	O	64.21 ± 43.51	45.80 ± 12.95	70.89 ± 3.97	52.70 ± 20.64	45.95 ± 6.43	47.33 ± 20.33
	C	$1.08x10^{10}$ ± $9.40x10^{9}$	$6.20x10^{9}$ ± $5.57x10^{9}$	$1.38x10^{10}$ ± $6.16x10^{8}$	$7.44x10^{9}$ ± $7.21x10^{9}$	$5.04x10^{9}$ ± $4.64x10^{9}$	$4.60x10^{9}$ ± $7.97x10^{9}$
V	O	691.72 ± 102.25	273.94 ± 52.60	243.82 ± 59.88	276.59 ± 17.85	174.19 ± 66.97	255.08 ± 35.78
	C	$3.68x10^{10}$ ± $2.20x10^{9}$	$2.66x10^{10}$ ± $2.08x10^{9}$	$2.54x10^{10}$ ± $2.63x10^{9}$	$2.68x10^{10}$ ± $5.67x10^{8}$	$2.17x10^{10}$ ± $4.98x10^{9}$	$2.60x10^{10}$ ± $1.64x10^{9}$
R	O	81.17 ± 20.97	50.75 ± 2.10	53.88 ± 6.89	53.05 ± 11.02	44.44 ± 10.17	59.20 ± 16.56
	C	$1.48x10^{10}$ ± $3.13x10^{9}$	$8.64x10^{9}$ ± $9.82x10^{9}$	$9.20x10^{9}$ ± $3.01x10^{9}$	$7.20x10^{9}$ ± $6.60x10^{9}$	$3.72x10^{9}$ ± $6.44x10^{9}$	$9.72x10^{9}$ ± $4.90x10^{9}$

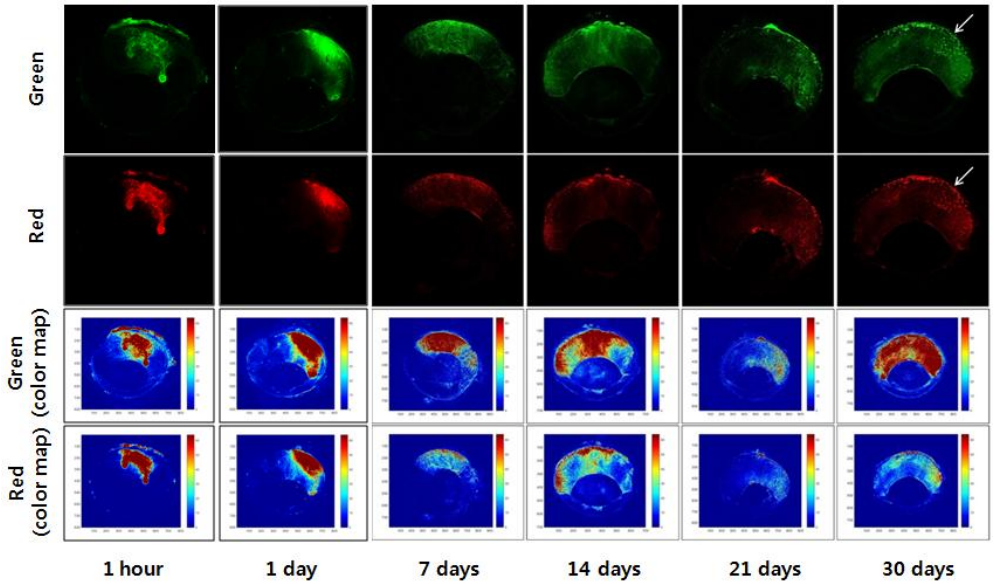

Figure 1. The intraocular distribution of nanoparticles over time following intravitreal injection in rabbit eyes. Numerous nanoparticles (white arrows) were observed in front of the retina at 30 days after the injection (green: 250 nm, red: 25 nm). The RGB images were obtained by using a MATLAB image processing toolbox.

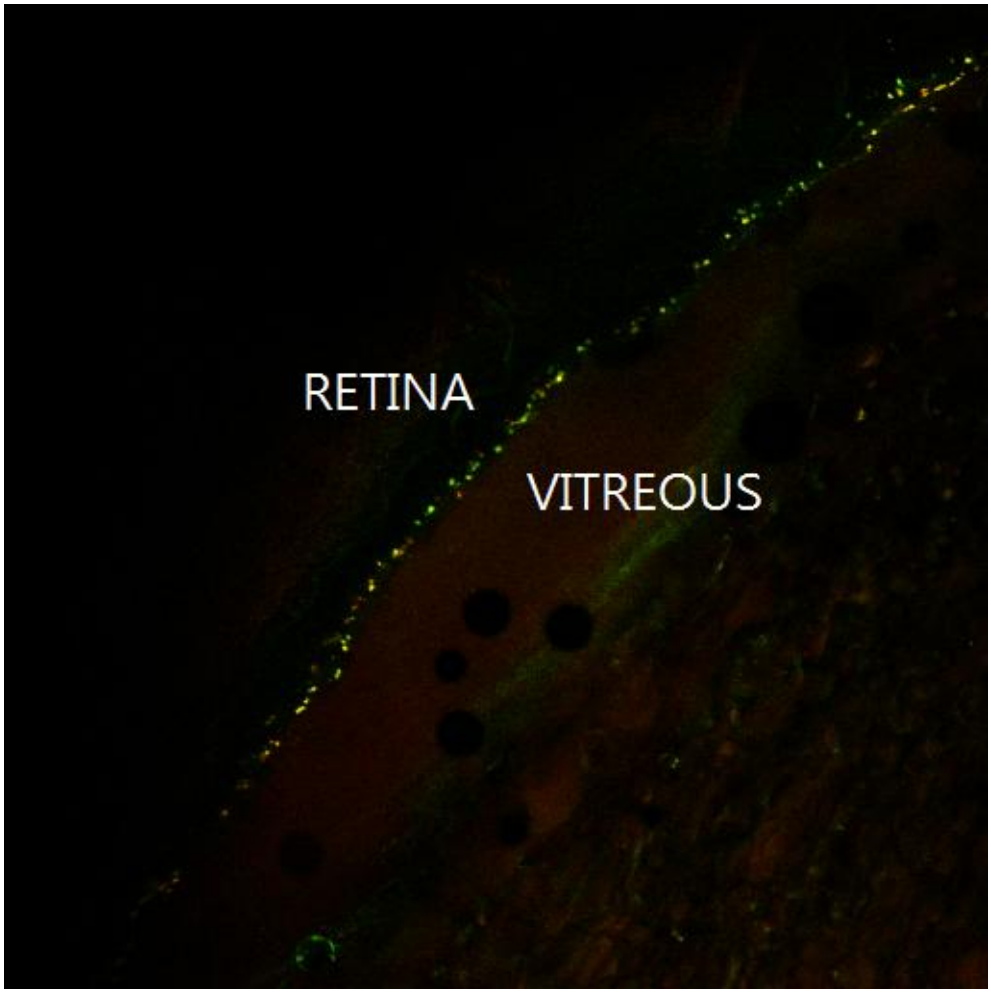

Figure 2. The retinal distribution of intravitreally injected nanoparticles (red color: 25 nm, green color: 250 nm).

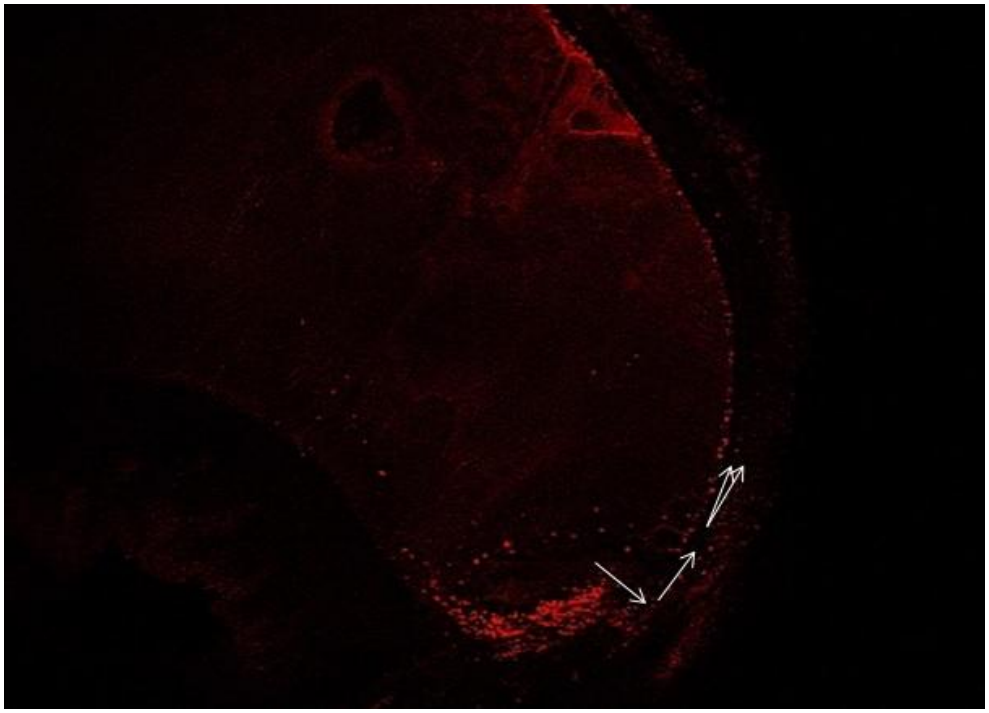

Figure 3. The movement of 25 nm nanoparticles (red color, white arrows) through the ciliary body into the choroid and episcleral space (The image was taken from an eye enucleated 21 days after the injection).

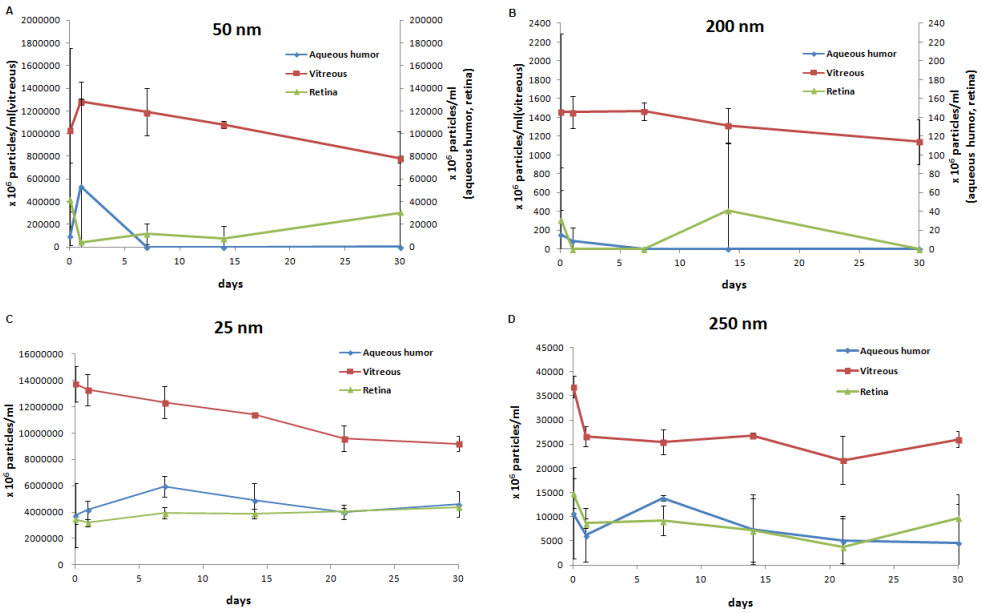

Figure 4. The average concentration (particles/ml) of nanoparticles in the aqueous humor, vitreous, and retina at 1 hour, 1 day, 7 days, 14 days, and 30 days (A, B) or 1 hour, 1 day, 7 days, 14 days, 21 days, and 30 days (C, D) after intravitreal nanoparticle injection (A: 50 nm, B: 200 nm, C: 25 nm, D: 250 nm).

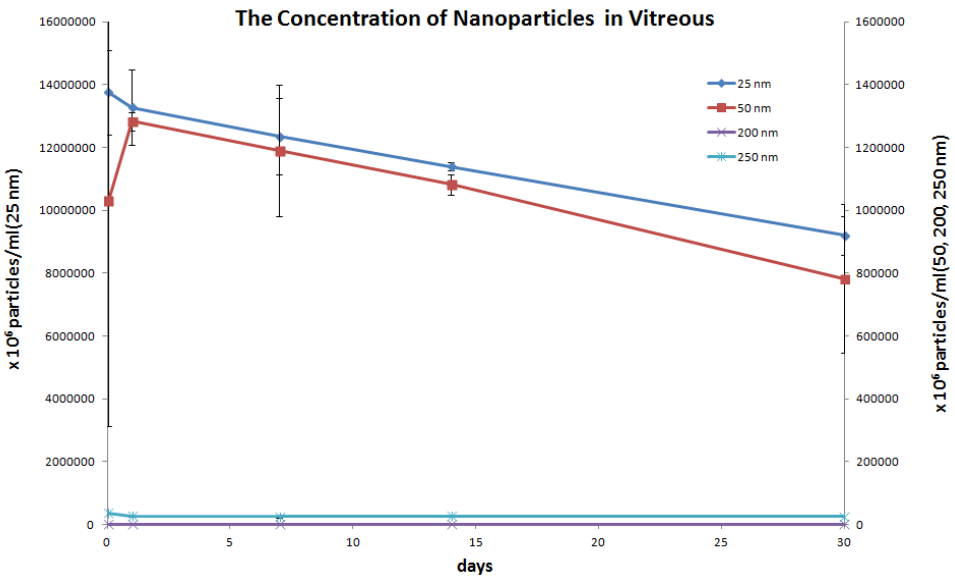

Figure 5. The average concentration (particles/ml) of nanoparticles in the vitreous at 1 hour, 1 day, 7 days, 14 days, and 30 days after intravitreal nanoparticle injection.

Discussion

We performed this study to analyze the distribution and kinetics of non-biodegradable nanoparticles after they were intravitreally injected into rabbit eyes.

1. Three main movement pathways of intravitreous nanoparticles

For a molecular probe placed in the vitreous, there are two major routes of elimination; through the retina or via the anterior route through the aqueous humor.[69] We found three main currents or movement pathways of intravitreally injected nanoparticles. The first pathway is where the nanoparticles move from the vitreous through the anterior chamber to the trabecular meshwork and it works at the early stage after intravitreal injection of the nanoparticles. The second pathway is where the nanoparticles move from the vitreous through the ciliary body into the choroid and episcleral space. The third pathway is where the nanoparticles move from the vitreous through the retina and choroid to the sclera. The first two pathways are related to the anterior movement of nanoparticles and the third is related to the posterior movement.

2. Distribution and kinetics in vitreous

We found that the intensity of fluorescence did not decrease in the vitreous over time and that 25 nm and 250 nm nanoparticles were not rapidly eliminated from the vitreous after they were injected intravitreally. We also found that 25 nm and 250 nm nanoparticles moved posteriorly to the retina from 7 days post-injection (Figure 1). We observed similar results with the kinetics of nanoparticles. The average concentration of nanoparticles, overall, did not change after 1 hour post-injection and this might reflect that, irrespective of their sizes, they were not rapidly eliminated (Tables 1~4, Figure 5).

Although the solid content of the vitreous humor is rare (~1%), the alignment of collagen and glycosaminoglycan is sufficient to maintain the rigidity and stability of the gel and more critically, acts as a molecular barrier to diffusion.[70] However, small molecules with low molecular weights encounter lower steric hindrance and hence their migration in the vitreous is largely diffusive.[71] Therefore, we think that the concentration of 25 nm and 50 nm nanoparticles decreased a little over time because they were smaller and might be distributed more easily.

The vitreous in a young rabbit eye is well formed and may be more effective in keeping the injected drug in a consolidated depot compared with the liquefied vitreous. A less consolidated depot may have an increase in surface area for drug dissolution and this may alter the pharmacokinetics of the drug.[43] It may also be

thought that 50 nm nanoparticles were more consolidated and could not move as easily as 200 nm nanoparticles because the 50 nm nanoparticle solution was less diluted when it was prepared for intravitreal injection. Nevertheless, smaller 50 nm nanoparticles were distributed more easily.

Sakurai et al. injected polystyrene nanospheres (2 μm, 200 nm, and 50 nm in diameter) containing a fluorescein derivative into the vitreous cavity of pigmented rabbit eyes and obtained the fluorescence intensity in the midvitreous.[65] They reported that the fluorescence intensity decreased with time in all three kinds and remained higher in smaller nanospheres than in larger nanospheres at 1 month after injection. The fluorescence was measured noninvasively by using a scanning fluorophotometer in the study. If the nanospheres kept moving posteriorly to the retina or accumulated on it, the detected fluorescence could decrease when they were detected with a fluorophotometer. The detected fluorescence could also decrease if the fluorescence itself decreased spontaneously although the number of nanoparticles did not decrease in the vitreous. We performed fluorescence microscopic imaging of enucleated eyes and could see the distribution of nanoparticles inside it. Moreover, we separated frozen vitreous from the eye and detected the fluorescence. Therefore, we think that our results could be closer to actual elimination of the injected nanoparticles.

As seen in figure 1, the intravitreally injected nanoparticles moved posteriorly

from 7 days after intravitreal injection. We can see a similar result in two studies analyzing the kinetics of protein drugs in the vitreous.[26,72] Although these studies did not analyze the distribution of nanoparticles, they might help us to infer the movement of nanoparticles since there are few studies about the distribution of nanoparticles. Ahn et al. also suggested that bevacizumab administered to the vitreous was mainly eliminated through the retina and choroid in the second slow elimination phase.[26] Park found that IgG and Fab began to migrate posteriorly to the retina from 1 day after the intravitreal injection. In the experiment, whole IgG antibodies and Fab fragments were injected intravitreally in the rabbit eyes to monitor the movement of bevacizumab and ranibizumab, which are commonly used anti-VEGF drugs for various retinal diseases, and serial imaging was conducted to track their movement over time.[72] Our results might show the distribution and elimination pathways of nanoparticles particularly well because non-biodegradable nanoparticles were used.

There has been controversy regarding the effect of vitrectomy on the pharmacokinetics of the vitreous. Since the vitreous is a gel consisting of aligned collagen and glycosaminoglycan, it has been thought to act as a molecular barrier to drug diffusion. Earlier studies have consistently shown vitrectomy to shorten the half-life of intravitreally injected materials such as VEGF and triamcinolone acetonide.[35,73]

Ahn et al. found that the elimination of bevacizumab in the vitreous consisted of two distinct phases and there was no substantial difference in the overall (1–30 days) pharmacokinetic properties of intravitreal bevacizumab in vitrectomized and nonvitrectomized control eyes. They suggested that any pharmacokinetic study without the 1-hour data would most likely overlook the first phase since the first fast distribution phase persists for only 1 day. Their second phase results showed different pharmacokinetic profiles, compared to that of the first phase, indicating a different elimination pathway such as to the posterior segment through the retina.[26] Ahn et al. also found that the pharmacokinetic properties of intravitreally administered ranibizumab in vitrectomized rabbit eyes were not substantially different from those in nonvitrectomized eyes. Vitrectomized and nonvitrectomized eyes showed similar concentrations of ranibizumab in the retina. They suggested that the role of the vitreous in the distribution and clearance of ranibizumab is insignificant and that similar dosing regimens for intravitreal ranibizumab injections may be used for patients that have previously received a vitrectomy.[30] The authors separated the frozen vitreous, aqueous humor, and retina from the eye and used an immunoassay, the most frequently used analytical method for assaying therapeutic proteins in biological samples. Therefore, they suggested that the results of their studies could show pharmacokinetic properties better than previous studies.[26,30]

In a study analyzing the pharmacokinetic profiles of intraocular VEGF-Trap, the

concentrations were highest in the aqueous humor and retina/choroid 1 hour after intravitreal administration, indicating that intravitreally injected VEGF-Trap rapidly distributes to the aqueous humor and retina/choroid. In addition, the VEGF-Trap concentrations in the aqueous humor and retina/choroid 1 hour post administration were about 60 and 30%, respectively, of the vitreous concentration. They suggested these results also indicate that the distribution and uptake to the retina/choroid from the vitreous may depend on the characteristics of each anti-VEGF agent, such as molecular weight, charge, glycosylation, and binding sites, which also affect the bioavailability of agents.[74]

The sum of the average concentration of nanoparticles in the vitreous, aqueous humor, and retina was different at each time point. We thought that the nanoparticles on the surface of the iris and lens might have affected the results of the kinetics according to the amount of them included in each sample. The fluorescence might have been underestimated. It was also possible that the nanoparticles had been eliminated through the anterior chamber.

3. Distribution and kinetics in anterior chamber

In figure 1, we found that the nanoparticles moved anteriorly in the vitreous at 1 hour and 1 day post-injection, and the fluorescence increased in the anterior chamber until 14 days after the injection and it decreased thereafter. The

concentration of 50 nm and 200 nm nanoparticles did not increase in the anterior chamber and the nanoparticles were not detected, or scarcely detected, from 1 day post-injection (Tables 1 and 2, Figure 4). The concentration of 25 nm and 250 nm nanoparticles did not increase in the anterior chamber from 7 days post-injection (Tables 3 and 4, Figure 4). Park found that IgG and Fab moved anteriorly until 1 day after the intravitreal injection and they began to move posteriorly thereafter.[72] Recent studies on the pharmacokinetic properties of anti-VEGF agents showed that their concentration in the aqueous humor peaked within 2 days after intravitreal injection.[26,30,74]

We thought that this may be because nanoparticles did not move to the anterior chamber from the vitreous after the early phase and nanoparticles that had migrated to the anterior chamber at the early phase were absorbed into the trabecular meshwork.

Another interesting finding is that 25 nm nanoparticles moved across the ciliary body into the choroid and episcleral space; shown in the image of the eye enucleated 21 days after the injection (Figure 3). We think this may be one route by which nanoparticles move from the vitreous to the choroid and episcleral space.

4. Distribution and kinetics in retina

In our study, nanoparticles could not penetrate into the deeper retinal structures

and accumulated on the internal limiting membrane (Figure 2). It has been suggested that the internal limiting membrane could form a diffusion barrier, particularly for large charged cationic species.[75] The inner limiting membrane is composed of a fine three-dimensional meshwork structure with numerous pores with sizes between 10 and 25 nm.[76,77] Therefore, we thought that 25 nm and 250 nm nanoparticles could not penetrate into the deeper retinal tissue.

Nanoparticles were detected in the retinal tissue (Tables 1~4, Figure 4). Although nanoparticles could not penetrate into the deeper retinal structures (Figure 2), it might be possible, not only because they accumulated on the internal limiting membrane, but because they might move to the choroid via the ciliary body and then move to the retina.

5. The strength and limitations of our study

We showed the distribution and kinetics of intravitreally injected non-biodegradable nanoparticles in rabbit eyes. Sakurai et al. also performed the study on the distribution and kinetics of intravitreally injected non-biodegradable nanoparticles in rabbit eyes.[65] However, we performed fluorescence microscopic imaging of enucleated eyes to see the actual distribution of intravitreally injected nanoparticles. While they measured the fluorescence in the midvitreous noninvasively by using a scanning fluorophotometer,[65] we separated the frozen

vitreous from the eye and detected the optical density of fluorescence. Moreover, they did not measure the fluorescence at 1 hour post-injection and therefore, our results could give more information about the kinetics at early phases.

There are some limitations to our study. First, the movement and kinetics of nanoparticles in human eyes are different from those in rabbit eyes. Compared to human eyes, the vitreous volume is smaller in the rabbit eyes (1.5 ml, approximately 40% of human vitreous volume) and the size of the crystal lens in relation to that of the whole eye is much larger in rabbits than in humans.[78] In addition, there is a possibility of different drug distribution mechanisms between human and rabbit eyes. Second, the nanoparticles on the surface of the iris and lens might have affected the kinetics of nanoparticles in each sample and the concentration of nanoparticles might have been underestimated if they were not included in each sample.

6. Future nanoparticles and drug delivery systems

Although nanoparticles and drug delivery systems have been developed continuously with the development of nanotechnology, there are only a few drugs and drug delivery systems that can be applicable for patients clinically. However, from the results of our study, we think that non-biodegradable nanoparticles or other forms of nanoparticles could be useful if they are improved upon and then used to

manufacture novel drug delivery systems in the future.

Conclusion

In conclusion, when the non-biodegradable nanoparticles were injected intravitreally, some of them were eliminated to the anterior chamber at the early phase and the rest remained in the vitreous cortex (vitreoretinal interface) for a long time. We could find three main currents or movement pathways of intravitreally injected nanoparticles. The first pathway is where the nanoparticles move from the vitreous through the anterior chamber to the trabecular meshwork and it works at the early phase after intravitreal injection of the the nanoparticles. The second pathway is where the nanoparticles move from the vitreous through the ciliary body into the choroid and episcleral space. The third pathway is where the nanoparticles move from the vitreous through the retina and choroid to the sclera. The first two pathways are related to the anterior movement of nanoparticles and the third is related to the posterior movement. However, the non-biodegradable nanoparticles could not penetrate the internal limiting membrane of the retina, thus long-term retention in the vitreous occurred.

In this study, we saw the intraocular distribution, changes in concentration, and elimination pathways of various-sized non-biodegradable nanoparticles. Particularly, we found that 25 nm nanoparticles could be eliminated directly through the ciliary body into the choroid and sclera; which is a novel finding. For these reasons, our

results may be used as basic data in the studies of intraocular drug delivery and pharmacokinetics using nanoparticles in the future. They might also indicate the possible mechanism of intraocular elimination and movement of intravitreally injected drugs, which are currently used to treat retinal diseases.

References

1. Hanout M, Ferraz D, Ansari M, et al. Therapies for neovascular age-related macular degeneration: current approaches and pharmacologic agents in development. BioMed Res Int. 2013;2013:830837.

2. Yau JWY, Rogers SL, Kawasaki R, et al. Global prevalence and major risk factors of diabetic retinopathy. Diabetes Care. 2012;35(3):556-64.

3. Klein R, Moss SE, Klein BE, Davis MD, DeMets DL. The Wisconsin epidemiologic study of diabetic retinopathy. XI. The incidence of macular edema. Ophthalmology. 1989;96(10):1501-10.

4. Mohamed Q, Gillies MC, Wong TY. Management of diabetic retinopathy: a systematic review. JAMA. 2007;298(8):902-16.

5. Hayreh SS. Classification of central retinal vein occlusion. Ophthalmology. 1983;90(5):458-74.

6. Natural history and clinical management of central retinal vein occlusion. The Central Vein Occlusion Study Group. Arch Ophthalmol. 1997;115(4):486-91.

7. Argon laser photocoagulation for macular edema in branch vein occlusion. The Branch Vein Occlusion Study Group. Am J Ophthalmol. 1984;98(3):271-82.

8. Brown DM, Campochiaro PA, Bhisitkul RB, et al. Sustained benefits from ranibizumab for macular edema following branch retinal vein occlusion: 12-month outcomes of a phase III study. Ophthalmology. 2011;118(8):1594-602.

9. Campochiaro PA, Brown DM, Awh CC, et al. Sustained benefits from ranibizumab for macular edema following central retinal vein occlusion: twelve-

month outcomes of a phase III study. Ophthalmology. 2011;118(10):2041-9.

10. Brown DM, Heier JS, Clark WL, et al. Intravitreal aflibercept injection for macular edema secondary to central retinal vein occlusion: 1-year results from the phase 3 COPERNICUS study. Am J Ophthalmol. 2013;155(3):429-37.e7.

11. Epstein DL, Algvere PV, von Wendt G, Seregard S, Kvanta A. Benefit from bevacizumab for macular edema in central retinal vein occlusion: twelve-month results of a prospective, randomized study. Ophthalmology. 2012;119(12):2587-91.

12. Ip MS, Scott IU, VanVeldhuisen PC, et al. A randomized trial comparing the efficacy and safety of intravitreal triamcinolone with observation to treat vision loss associated with macular edema secondary to central retinal vein occlusion: the Standard Care vs Corticosteroid for Retinal Vein Occlusion (SCORE) study report 5. Arch Ophthalmol. 2009;127(9):1101-14.

13. Massin P, Bandello F, Garweg JG, et al. Safety and efficacy of ranibizumab in diabetic macular edema (RESOLVE Study): a 12-month, randomized, controlled, double-masked, multicenter phase II study. Diabetes Care. 2010;33(11):2399-405.

14. Nguyen QD, Brown DM, Marcus DM, et al. Ranibizumab for diabetic macular edema: results from 2 phase III randomized trials: RISE and RIDE. Ophthalmology. 2012;119(4):789-801.

15. Rajendram R, Fraser-Bell S, Kaines A, et al. A 2-year prospective randomized controlled trial of intravitreal bevacizumab or laser therapy (BOLT) in the management of diabetic macular edema: 24-month data: report 3. Arch Ophthalmol. 2012;130(8):972-9.

16. Michaelides M, Kaines A, Hamilton RD, et al. A prospective randomized trial of intravitreal bevacizumab or laser therapy in the management of diabetic macular edema (BOLT study) 12-month data: report 2. Ophthalmology. 2010;117(6):1078-86.e2.

17. Lam DSC, Lai TYY, Lee VYW, et al. Efficacy of 1.25 MG versus 2.5 MG intravitreal bevacizumab for diabetic macular edema: six-month results of a randomized controlled trial. Retina Phila Pa. 2009;29(3):292-9.

18. Arevalo JF, Sanchez JG, Wu L, et al. Primary intravitreal bevacizumab for diffuse diabetic macular edema: the Pan-American Collaborative Retina Study Group at 24 months. Ophthalmology. 2009;116(8):1488-97, 1497.e1.

19. Do DV, Schmidt-Erfurth U, Gonzalez VH, et al. The DA VINCI Study: phase 2 primary results of VEGF Trap-Eye in patients with diabetic macular edema. Ophthalmology. 2011;118(9):1819-26.

20. Do DV, Nguyen QD, Boyer D, et al. One-year outcomes of the da Vinci Study of VEGF Trap-Eye in eyes with diabetic macular edema. Ophthalmology. 2012;119(8):1658-65.

21. Jonas JB, Kamppeter BA, Harder B, Vossmerbaeumer U, Sauder G, Spandau UHM. Intravitreal triamcinolone acetonide for diabetic macular edema: a prospective, randomized study. J Ocul Pharmacol Ther Off J Assoc Ocul Pharmacol Ther. 2006;22(3):200-7.

22. Audren F, Erginay A, Haouchine B, et al. Intravitreal triamcinolone acetonide for diffuse diabetic macular oedema: 6-month results of a prospective controlled

trial. Acta Ophthalmol Scand. 2006;84(5):624-30.

23. Gillies MC, Sutter FKP, Simpson JM, Larsson J, Ali H, Zhu M. Intravitreal triamcinolone for refractory diabetic macular edema: two-year results of a double-masked, placebo-controlled, randomized clinical trial. Ophthalmology. 2006;113(9):1533-8.

24. Khan M, Agarwal K, Loutfi M, Kamal A. Present and possible therapies for age-related macular degeneration. ISRN Ophthalmol. 2014;2014:608390.

25. Maurice D. Review: practical issues in intravitreal drug delivery. J Ocul Pharmacol Ther Off J Assoc Ocul Pharmacol Ther. 2001;17(4):393-401.

26. Ahn J, Kim H, Woo SJ, et al. Pharmacokinetics of intravitreally injected bevacizumab in vitrectomized eyes. J Ocul Pharmacol Ther Off J Assoc Ocul Pharmacol Ther. 2013;29(7):612-8.

27. Nomoto H, Shiraga F, Kuno N, et al. Pharmacokinetics of bevacizumab after topical, subconjunctival, and intravitreal administration in rabbits. Invest Ophthalmol Vis Sci. 2009;50(10):4807-13.

28. Sinapis CI, Routsias JG, Sinapis AI, et al. Pharmacokinetics of intravitreal bevacizumab (Avastin®) in rabbits. Clin Ophthalmol Auckl NZ. 2011;5:697-704.

29. Bakri SJ, Snyder MR, Reid JM, Pulido JS, Singh RJ. Pharmacokinetics of intravitreal bevacizumab (Avastin). Ophthalmology. 2007;114(5):855-9.

30. Ahn SJ, Ahn J, Park S, et al. Intraocular pharmacokinetics of ranibizumab in vitrectomized versus nonvitrectomized eyes. Invest Ophthalmol Vis Sci. 2014;55(1):567-73.

31. Bakri SJ, Snyder MR, Reid JM, Pulido JS, Ezzat MK, Singh RJ. Pharmacokinetics of intravitreal ranibizumab (Lucentis). Ophthalmology. 2007;114(12):2179-82.

32. Gaudreault J, Fei D, Beyer JC, et al. Pharmacokinetics and retinal distribution of ranibizumab, a humanized antibody fragment directed against VEGF-A, following intravitreal administration in rabbits. Retina Phila Pa. 2007;27(9):1260-6.

33. Gaudreault J, Fei D, Rusit J, Suboc P, Shiu V. Preclinical pharmacokinetics of Ranibizumab (rhuFabV2) after a single intravitreal administration. Invest Ophthalmol Vis Sci. 2005;46(2):726-33.

34. Christoforidis JB, Williams MM, Kothandaraman S, Kumar K, Epitropoulos FJ, Knopp MV. Pharmacokinetic properties of intravitreal I-124-aflibercept in a rabbit model using PET/CT. Curr Eye Res. 2012;37(12):1171-4.

35. Chin H-S, Park T-S, Moon Y-S, Oh J-H. Difference in clearance of intravitreal triamcinolone acetonide between vitrectomized and nonvitrectomized eyes. Retina Phila Pa. 2005;25(5):556-60.

36. Beer PM, Bakri SJ, Singh RJ, Liu W, Peters GB, Miller M. Intraocular concentration and pharmacokinetics of triamcinolone acetonide after a single intravitreal injection. Ophthalmology. 2003;110(4):681-6.

37. Oishi M, Maeda S, Hashida N, Ohguro N, Tano Y, Kurokawa N. Pharmacokinetic behavior of intravitreal triamcinolone acetonide prepared by a hospital pharmacy. Jpn J Ophthalmol. 2008;52(6):489-92.

38. Ye Y-F, Gao Y-F, Xie H-T, Wang H-J. Pharmacokinetics and retinal toxicity of

various doses of intravitreal triamcinolone acetonide in rabbits. Mol Vis. 2014;20:629-36.

39. Moisseiev E, Waisbourd M, Ben-Artsi E, et al. Pharmacokinetics of bevacizumab after topical and intravitreal administration in human eyes. Graefes Arch Clin Exp Ophthalmol Albrecht Von Graefes Arch Für Klin Exp Ophthalmol. 2014;252(2):331-7.

40. Chu KO, Liu DTL, Chan KP, et al. Quantification and structure elucidation of in vivo bevacizumab modification in rabbit vitreous humor after intravitreal injection. Mol Pharm. 2012;9(12):3422-33.

41. Abd-El-Barr MM, Albini TA, Carvounis PE, et al. Safety and pharmokinetics of triamcinolone hexacetonide in rabbit eyes. J Ocul Pharmacol Ther Off J Assoc Ocul Pharmacol Ther. 2008;24(2):197-205.

42. Christoforidis JB, Xie Z, Jiang A, et al. Serum levels of intravitreal bevacizumab after vitrectomy, lensectomy and non-surgical controls. Curr Eye Res. 2013;38(7):761-6.

43. Kim H, Csaky KG, Gravlin L, et al. Safety and pharmacokinetics of a preservative-free triamcinolone acetonide formulation for intravitreal administration. Retina Phila Pa. 2006;26(5):523-30.

44. Eckardt C, Nicolai U, Czank M, Schmidt D. [Ocular tissue after intravitreous silicone oil injection. Histologic and electron microscopy studies]. Ophthalmol Z Dtsch Ophthalmol Ges. 1993;90(3):250-7.

45. Gambrelle J, Kodjikian L, Abi-Ayad N, Wolff B, Grange JD. [Persistent

unsealed sclerotomy after intravitreal injection of triamcinolone acetonide with a 30-gauge needle]. J Fr Ophtalmol. 2006;29(9):e22.

46. Zarbin MA, Montemagno C, Leary JF, Ritch R. Nanomedicine in ophthalmology: the new frontier. Am J Ophthalmol. 2010;150(2):144-62.e2.

47. Morrow KJ, Bawa R, Wei C. Recent advances in basic and clinical nanomedicine. Med Clin North Am. 2007;91(5):805-43.

48. Giarmoukakis A, Labiris G, Sideroudi H, et al. Biodegradable nanoparticles for controlled subconjunctival delivery of latanoprost acid: in vitro and in vivo evaluation. Preliminary results. Exp Eye Res. 2013;112:29-36.

49. Tuomela A, Liu P, Puranen J, et al. Brinzolamide nanocrystal formulations for ophthalmic delivery: reduction of elevated intraocular pressure in vivo. Int J Pharm. 2014;467(1-2):34-41.

50. Gagandeep null, Garg T, Malik B, Rath G, Goyal AK. Development and characterization of nano-fiber patch for the treatment of glaucoma. Eur J Pharm Sci Off J Eur Fed Pharm Sci. 2014;53:10-6.

51. Singh J, Chhabra G, Pathak K. Development of acetazolamide-loaded, pH-triggered polymeric nanoparticulate in situ gel for sustained ocular delivery: in vitro. ex vivo evaluation and pharmacodynamic study. Drug Dev Ind Pharm. 2014;40(9):1223-32.

52. Pisal PB, Joshi MA, Padamwar MN, Patil SS, Pokharkar VB. Probing influence of methodological variation on active loading of acetazolamide into nanoliposomes: biophysical, in vitro, ex vivo, in vivo and rheological investigation. Int J Pharm.

2014;461(1-2):82-8.

53. Natarajan JV, Darwitan A, Barathi VA, et al. Sustained drug release in nanomedicine: a long-acting nanocarrier-based formulation for glaucoma. ACS Nano. 2014;8(1):419-29.

54. Guha R, Chowdhury S, Palui H, et al. Doxorubicin-loaded MePEG-PCL nanoparticles for prevention of posterior capsular opacification. Nanomed. 2013;8(9):1415-28.

55. Kaiser JM, Imai H, Haakenson JK, et al. Nanoliposomal minocycline for ocular drug delivery. Nanomedicine Nanotechnol Biol Med. 2013;9(1):130-40.

56. Kim H, Csaky KG. Nanoparticle-integrin antagonist C16Y peptide treatment of choroidal neovascularization in rats. J Control Release Off J Control Release Soc. 2010;142(2):286-93.

57. Araújo J, Gonzalez-Mira E, Egea MA, Garcia ML, Souto EB. Optimization and physicochemical characterization of a triamcinolone acetonide-loaded NLC for ocular antiangiogenic applications. Int J Pharm. 2010;393(1-2):167-75.

58. Hirani A, Grover A, Lee YW, Pathak Y, Sutariya V. Triamcinolone acetonide nanoparticles incorporated in thermoreversible gels for age-related macular degeneration. Pharm Dev Technol. September 2014:1-7.

59. Das S, Suresh PK. Nanosuspension: a new vehicle for the improvement of the delivery of drugs to the ocular surface. Application to amphotericin B. Nanomedicine Nanotechnol Biol Med. 2011;7(2):242-7.

60. Robinson R, Viviano SR, Criscione JM, et al. Nanospheres delivering the EGFR

TKI AG1478 promote optic nerve regeneration: the role of size for intraocular drug delivery. ACS Nano. 2011;5(6):4392-400.

61. Sabzevari A, Adibkia K, Hashemi H, et al. Improved anti-inflammatory effects in rabbit eye model using biodegradable poly beta-amino ester nanoparticles of triamcinolone acetonide. Invest Ophthalmol Vis Sci. 2013;54(8):5520-6.

62. Rafie F, Javadzadeh Y, Javadzadeh AR, et al. In vivo evaluation of novel nanoparticles containing dexamethasone for ocular drug delivery on rabbit eye. Curr Eye Res. 2010;35(12):1081-9.

63. Sabzevari A, Adibkia K, Hashemi H, et al. Polymeric triamcinolone acetonide nanoparticles as a new alternative in the treatment of uveitis: in vitro and in vivo studies. Eur J Pharm Biopharm Off J Arbeitsgemeinschaft Für Pharm Verfahrenstechnik EV. 2013;84(1):63-71.

64. Amrite AC, Edelhauser HF, Singh SR, Kompella UB. Effect of circulation on the disposition and ocular tissue distribution of 20 nm nanoparticles after periocular administration. Mol Vis. 2008;14:150-60.

65. Sakurai E, Ozeki H, Kunou N, Ogura Y. Effect of particle size of polymeric nanospheres on intravitreal kinetics. Ophthalmic Res. 2001;33(1):31-6.

66. Inokuchi Y, Hironaka K, Fujisawa T, et al. Physicochemical properties affecting retinal drug/coumarin-6 delivery from nanocarrier systems via eyedrop administration. Invest Ophthalmol Vis Sci. 2010;51(6):3162-70.

67. Hwang Y, Ahn J, Mun J, et al. In vivo analysis of THz wave irradiation induced acute inflammatory response in skin by laser-scanning confocal microscopy. Opt

Express. 2014;22(10):11465-75.

68. Choe K, Jang JY, Park I, et al. Intravital imaging of intestinal lacteals unveils lipid drainage through contractility. J Clin Invest. 2015;125(11):4042-52.

69. Maurice DM. Injection of drugs into the vitreous body. In: Symposium on Ocular Therapy. Vol 9. John Wiley and Sons, Inc. New York; 1976:59–72.

70. Laude A, Tan LE, Wilson CG, et al. Intravitreal therapy for neovascular age-related macular degeneration and inter-individual variations in vitreous pharmacokinetics. Prog Retin Eye Res. 2010;29(6):466-75.

71. Park J, Bungay PM, Lutz RJ, et al. Evaluation of coupled convective-diffusive transport of drugs administered by intravitreal injection and controlled release implant. J Control Release Off J Control Release Soc. 2005;105(3):279-95.

72. Park S. Movements and Pharmacokinetics of intravitreally injected antibody. Master's Dissertation. Sogang University, Seoul, Republic of Korea. 2013.

73. Lee SS, Ghosn C, Yu Z, et al. Vitreous VEGF clearance is increased after vitrectomy. Invest Ophthalmol Vis Sci. 2010;51(4):2135-8.

74. Park SJ, Oh J, Kim Y-K, et al. Intraocular pharmacokinetics of intravitreal vascular endothelial growth factor-Trap in a rabbit model. Eye Lond Engl. 2015;29(4):561-8.

75. Pitkänen L, Pelkonen J, Ruponen M, Rönkkö S, Urtti A. Neural retina limits the nonviral gene transfer to retinal pigment epithelium in an in vitro bovine eye model. AAPS J. 2004;6(3):e25.

76. Nishihara H. [Studies on the ultrastructure of the inner limiting membrane of the

retina. I. Surface replication study on the inner limiting membrane of the retina]. Nippon Ganka Gakkai Zasshi. 1989;93(4):429-38.

77. Nishihara H. [Studies on the ultrastructure of the inner limiting membrane of the retina--distribution of anionic sites in the inner limiting membrane of the retina]. Nippon Ganka Gakkai Zasshi. 1991;95(10):951-8.

78. Short BG. Safety evaluation of ocular drug delivery formulations: techniques and practical considerations. Toxicol Pathol. 2008;36(1):49-62.

국문 초록

서론: 최근 많은 망막 질환들의 치료를 위해 거대 단백질 약물들이 유리체강내로 주사되고 있는데, 분자량이 동력학을 결정하는데 있어서 주요 인자로 알려져 있지만, 약물전달, 안구내 분포와 제거의 정확한 기전에 대해서는 잘 알려져 있지 않다. 나노입자를 포함한 다양한 종류의 약물전달시스템들이 안구 조직에 약물전달을 향상시키고자 개발되어 왔다. 이번 연구는 백색 가토의 안구에 비생분해성 나노입자를 유리체강내로 주사한 후 안구내 분포와 동력학을 분석하여 유리체내의 물질과 약물의 안구내 생물학적 분포를 이해하는데 도움을 주고자 시행되었다.

방법: 형광물질이 부착된 비생분해성 폴리스티렌 나노입자 제품들이 실험에 사용되었다. 지름 25 nm 나노입자 용액과 지름 250 nm 나노입자 용액을 1:1의 비율로 혼합하여 0.034 ml를 12마리의 백색 가토 양안에 유리체강내 주사하였다. 주사 후 1시간 뒤, 1일 뒤, 7일 뒤, 14일 뒤, 21일 뒤, 30일 뒤, 각 시기별로 4안씩 안구적출을 하여 섭씨 영하 80도에 보관하였다. 이 중에서 각 시기별로 1안을 이용하여 안구 단면의 형광 이미징을 시행하였다. 자체 제작한 레이저 주사 공초점 현미경(Custom-built laser-scanning confocal system)을 광각

영상(wide-field imaging)이 가능하도록 변경하여 냉동 상태인 안구가 녹기 시작하기 전에 적출 안구 단면의 형광 현미경 이미징을 시행한 후, 소프트웨어를 이용하여 시간대별로 나노입자의 안구내 분포를 분석하였다. 나머지 18안의 냉동 보관된 안구를 해체하여 방수, 유리체, 망막 조직을 채취한 후 형광 microplate reader를 이용하여 각 조직의 형광물질에 대한 흡광도를 측정하고 이를 이용하여 각 조직 내에 들어있는 나노입자의 농도를 결정하였다. 지름 50 nm 나노입자 용액과 지름 200 nm 나노입자 용액을 각각 10배, 100배 희석하여, 제품당 0.05 ml를 각각 15마리의 백색 가토 우안에 유리체강내 주사하였다. 주사 후 1시간 뒤, 1일 뒤, 7일 뒤, 14일 뒤, 30일 뒤, 각 시기별로 3안씩 안구적출을 하여 섭씨 영하 80도에 보관하였다. 냉동 보관된 안구를 해체하여 방수, 유리체, 망막 조직을 채취한 후, 같은 방법으로 각 조직 내에 들어있는 나노입자의 농도를 결정하였다.

결과: 나노입자의 안구내 분포에 관한 순차적 이미징에서 유리체내 형광의 강도는 시간이 지나도 감소하지 않는 것을 볼 수 있었고, 유리체강내로 주사된 나노입자는 주사 후 7 일 이후부터 안구의 뒤쪽인 망막 쪽으로 이동한 것을 볼 수 있었다. 그러나, 나노입자는 망막을 뚫고 들어가지 못하고, 내경계막에 모여 있었다. 주사 후 1 시간째와 1 일째에 유리체내에서 나노입자들이 안구의 앞쪽으로 이동하는 것과 주사 후 14 일까지 전방에서 형광이 증가되고 이후 감소하는 것을 관찰할 수

있었다. 주사 후 21 일째에 적출된 안구의 이미지에서 나노입자들이 모양체를 가로질러 맥락막과 공막바깥공간으로 이동하는 것을 볼 수 있었다. 나노입자들의 유리체 농도는 시간이 지나도 큰 감소 없이 모든 측정 시간대에 잘 유지가 되었다. 전방에서 50 nm 나노입자와 200 nm 나노입자의 농도는 주사 후 1 일 이후, 25 nm 나노입자와 250 nm 나노입자의 농도는 주사 후 7 일 이후에는 증가하지 않았다. 망막에서 모든 종류의 나노입자들이 농도가 측정되었다.

결론: 유리체강내로 주입된 비생분해성 나노입자의 안구내 분포와 농도 변화, 제거 경로들에 대한 본 연구의 결과는 향후 나노입자를 이용한 약물전달과 약동학 연구에 기초 자료로 활용될 수 있을 것으로 생각되고, 현재 망막 질환의 치료에 사용되는 약물들을 유리체강내로 주입하였을 때 안구내 제거와 운동의 가능한 기전을 보여줄 수 있을 것으로 생각된다.

주요어: 나노입자, 유리체강내 주사, 안구내 분포, 동력학

학 번: 2010-30553